

NUMERICAL MODELING OF SOIL-STRUCTURE INTERACTION WITH APPLICATIONS TO GEOSYNTHETICS

Mahmoud G. Hussein¹ and Mohamed A. Meguid²

*¹ Ph.D. Candidate, ² Associate Professor of Geotechnical Engineering
Department of Civil Engineering and Applied Mechanics,
McGill University, Montreal, Quebec, Canada H3A 0C3*

ABSTRACT

Finite element method has proven to be a powerful tool in modelling boundary value problems, particularly those involving soil-structure interaction. Incorporating geosynthetics in civil engineering projects is rapidly growing, especially in the design of earth supported structures. Applications include reinforced earth fills, retaining walls, embankments, buried structures and shallow foundations. In this study, 2D and 3D finite element analyses are conducted using ABAQUS software to investigate two different soil-structure interaction problems: 1) three-dimensional analysis of unconfined and soil-confined geogrid with an example of a square footing over geogrid-reinforced soil, 2) two-dimensional plane strain analysis of a box culvert overlain by EPS geofoam inclusion to reduce earth pressure on the walls of the structure. Validation is performed by comparing the FE results with experimental data. Conclusions are made regarding the effectiveness of using the finite element method to solve these classes of geotechnical engineering problems.

Keywords: soil-geogrid interaction, finite element, reinforced soil, EPS geofoam

INTRODUCTION

Numerical modeling of soil-structure interaction problems involving flexible or soft geosynthetic inclusions is known to be challenging, especially in the presence of nearby rigid structures. This is attributed to the complicated nature of the created soil-geosynthetic-structure system with different material models and interaction behavior. Analyzing the problem using continuum approaches (e.g. finite element method) consists of finding a unique system of displacements for each component that satisfies both force equilibrium and material continuity. The objective of this study is to present a numerical approach that has been successfully used to model two different soil-structure interaction problems with geosynthetics inclusion. The steps taken in modelling the response of each involved material and interaction details are summarized. The results of this numerical investigation allowed for the merits of using geosynthetic material in two practical applications to be investigated.

GEOGRID-REINFORCED SOILS

Geogrid reinforcement is known to be an effective method to enhance the performance of earth structures (e.g. embankments, foundations and retaining walls). Reinforced soil structures are routinely designed using limit equilibrium methods. These methods do not generally provide sufficient information on the failure load and the strains developing in the reinforcement [1, 2]. On the other hand, numerical methods have become powerful tools to efficiently calculate the pre-failure displacements, and stresses in the reinforcement material. Several studies that employ finite and discrete element methods to analyze geogrid-reinforced structures have been reported in the literature [3-8]. Most of these studies focused on the overall response of the reinforced structure while adopting simplifying assumptions related to either the details of the geogrid geometry or the constitutive model of the geogrid material.

Modeling Unconfined Geogrid

In this section a 3D elasto-plastic FE model is developed using the general finite element software ABAQUS, version 6.13 [9], to simulate the behavior of unconfined geogrid under tensile loading. A series of index tests involving uniaxial-tensile loading was initially performed to measure the load-displacement response of biaxial geogrid samples. The tests are conducted on multi-rib geogrid specimens in both the machine (MD) and the cross machine (XMD) directions. The geogrid properties as provided by the manufacturer are summarized in Table 1.

Table 1: Index properties of the biaxial geogrid

Direction	Aperture size (mm)	Specimen size (mm)		No. of members		Ult. strength (kN/m)	Mass/ unit area (g/m ²)	Stiffness @ 2% strain (kN/m)
		L	W	Long.	Trans.			
MD	29	149	78	3	6	12	215	204
XMD	37	185	58			20		292

The directional load-strain response of the tested geogrid is presented in Fig. 1. The geogrid response is found to be mostly nonlinear with significant plastic deformations as failure is approached.

Model development and validation

Three-dimensional FE analyses are conducted to simulate the index tests considering the geometric features and the nonlinear behavior of the geogrid. The different model components are listed below.

Geometry and boundary conditions: The details of the true geometry of the geogrid (Fig. 2) are explicitly simulated considering the thicknesses of different elements and the aperture structure.

Geogrid material model: Experimental results showed that biaxial geogrid behaves as a nonlinear elasto-plastic hardening material. Although the tested biaxial geogrid exhibited different responses in the MD and XMD, the experimental results showed that the degree of anisotropy in both the elastic and the plastic regimes is small, and therefore the anisotropy of the biaxial geogrid is not explicitly considered in this study. Alternatively, an average stress-strain relationship that represents a state between the

MD and the XMD responses (Fig. 1) is adopted. The constitutive model that is capable of simulating the nonlinear elastic, isotropic hardening plastic material is built using ABAQUS software package. The elasticity component of the geogrid model is described by an elastic isotropic model with a Young’s modulus value of 605MPa and a Poisson’s ratio of 0.3. The plasticity is modeled using Mises yield criterion with isotropic hardening and associated flow rule.

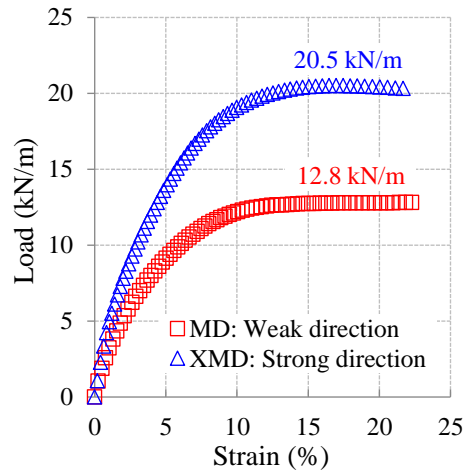


Figure 1. Experimental load-strain results of unconfined geogrid

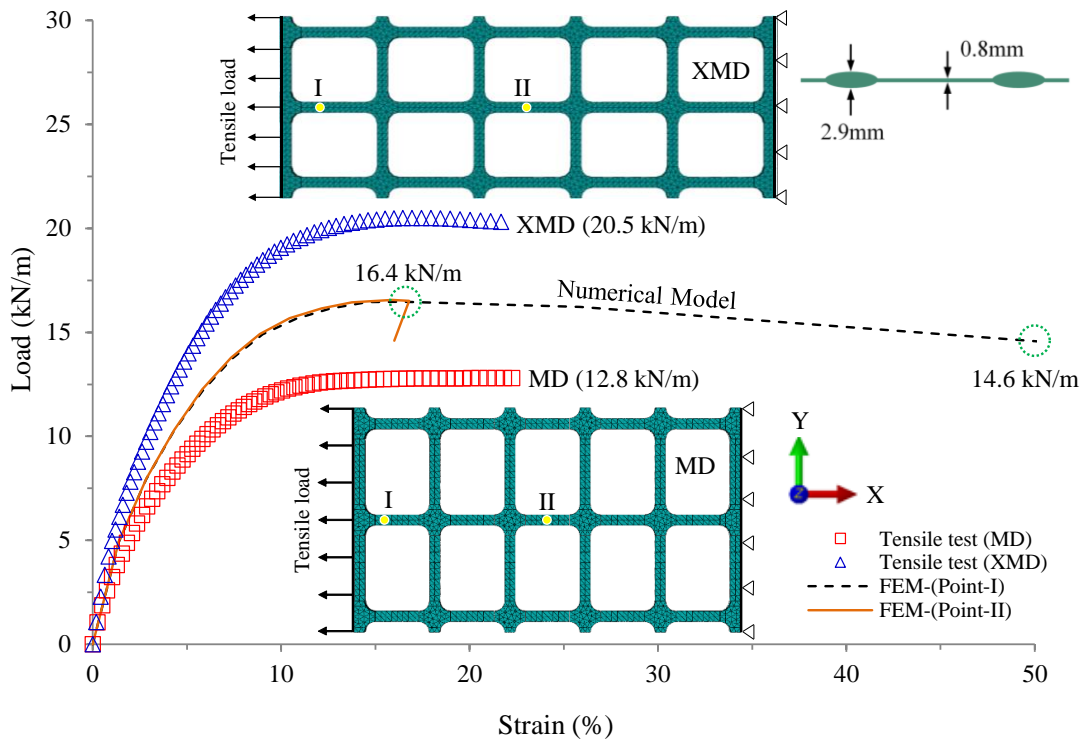


Figure 2. Experimental versus calculated results of unconfined geogrid

To validate the proposed 3D FE model for unconfined geogrid, the geogrid specimen is simulated using 8-node continuum linear brick elements (C3D8). The calculated and measured load-strain relationships are compared in Fig. 2. Two reference points located on the longitudinal ribs are used to illustrate the geogrid response. The calculated stress-strain response represents an average state between the measured values in the MD and

XMD. A maximum tensile load of 16.4 kN/m was generally reached at about 14% strain. Point (I) experienced significant strain with a slow rate of decrease in tensile load before failure. The tensile load at point (II) followed a similar path up to 16% strain where the load dropped rapidly from 16.4 to 14.6 kN/m.

Displacement and stresses in the geogrid

The deformed shape and displacement pattern along the geogrid are illustrated in Fig. 3a for an applied boundary displacement (U_x) of 23 mm (onset of necking). Displacements generally decreased with distance from the applied load (left side) and reached zero at the fixed boundary. The stress distribution within the geogrid is also shown in Fig. 3a. In contrast with the displacement pattern, the stresses in the loading direction (S_{xx}) were found to be almost uniform along the longitudinal ribs. Much smaller stress changes were calculated in the transverse bars as well as at the connecting junctions. Fig. 3a is also giving the equivalent plastic strains (PEEQ) developing in the geogrid under the applied tensile loads. It is evident that plastic strains are concentrated within the necking zone located near the applied load.

The patterns observed in Fig. 3a are confirmed by plotting the normalized displacements along the geogrid as shown in Fig. 3b. Displacement values were found to decrease linearly with distance from the applied load. The stress distribution (Fig. 3c) shows that the longitudinal ribs carry most of the applied load with only about one fourth of the load felt by the junctions. The load transferred to the transverse bars was found to be negligible.

Modeling a Square Footing on Geogrid-Reinforced Soil

The experimental results reported by Chen et al. [10] for square footing supported by geogrid-reinforced crushed limestone is used to validate the proposed geogrid model. The experiments investigated the stress distribution in the soil mass with and without reinforcement as well as the strains developing in the geogrid. The model footing used in the tests was 1 in. thick steel plate with dimensions of 152 mm \times 152 mm placed at the center of a rigid container (1.5 m \times 0.91 m \times 0.91 m). The soil used in the experiment was Kentucky crushed limestone with maximum dry unit weight of 22.68 kN/m³, and a peak friction angle of 53°. The elastic modulus of the crushed limestone was estimated from triaxial tests to be 120 MPa. Biaxial geogrids similar to that used in this study (Table 1) with dimensions of 1.5 m in length and 0.9 m in width were used in the experiments. The upper geogrid layer was installed at a depth of 50 mm below the foundation base. The number of geogrid layers installed in the soil was varied keeping a distance of 50 mm between two overlying geogrid layers.

Details of the numerical model

The numerical models used for the analysis of reinforced and unreinforced soils have been developed following the geometry and test procedure used in the experiments. The analysis is performed for up to two geogrid layers. It should be noted that only one-quarter of the geometry has been modeled to take advantage of the symmetry as shown in Fig. 4.

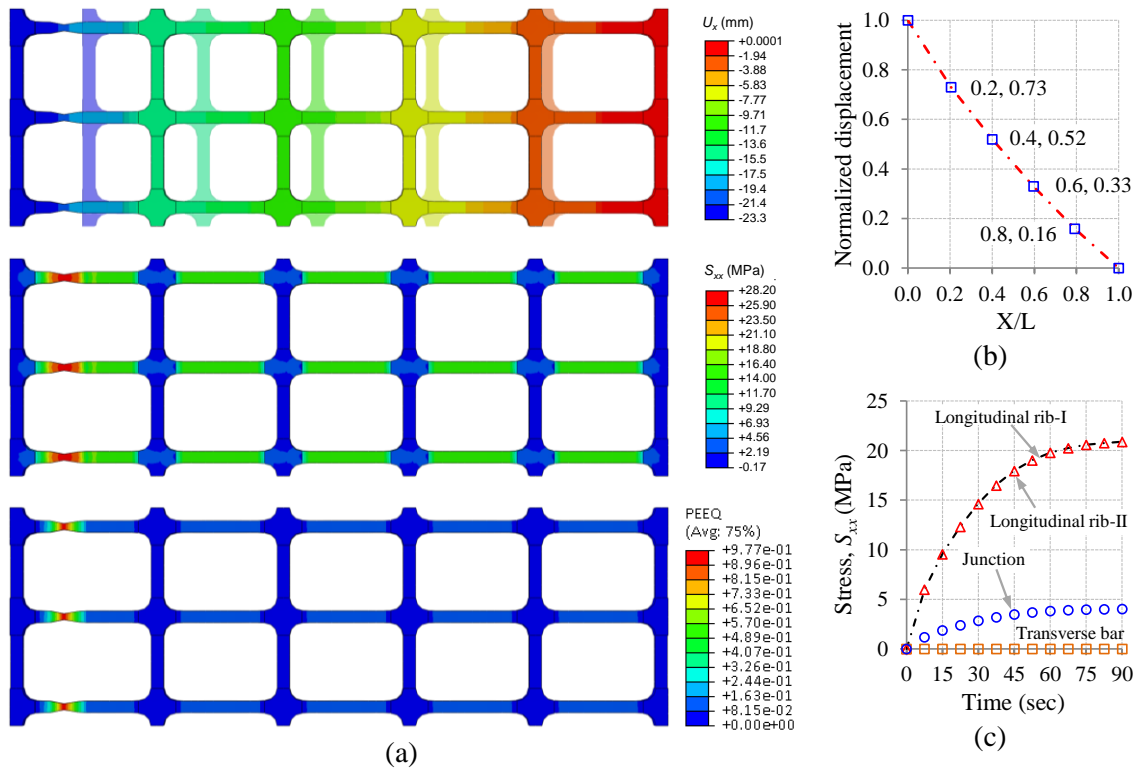


Figure 3. a) Deformed geogrid at $U_x = 23$ mm in the XMD
 b) Displacement distribution with distance from loaded boundary
 c) Stress transfer along the geogrid

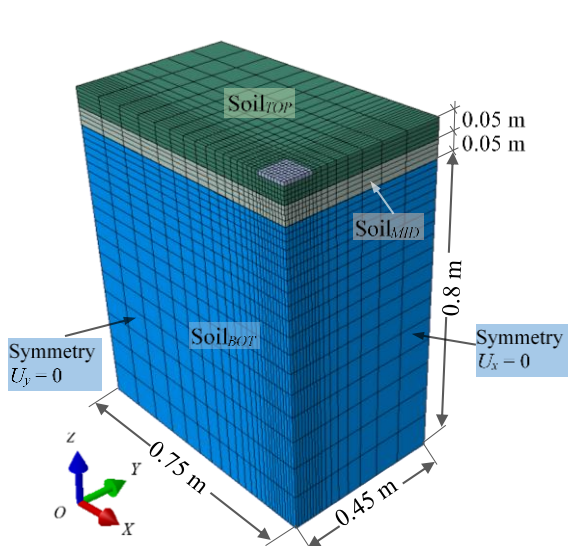


Figure 4. Complete 3D mesh geometry of the soil-confined geogrid FE model

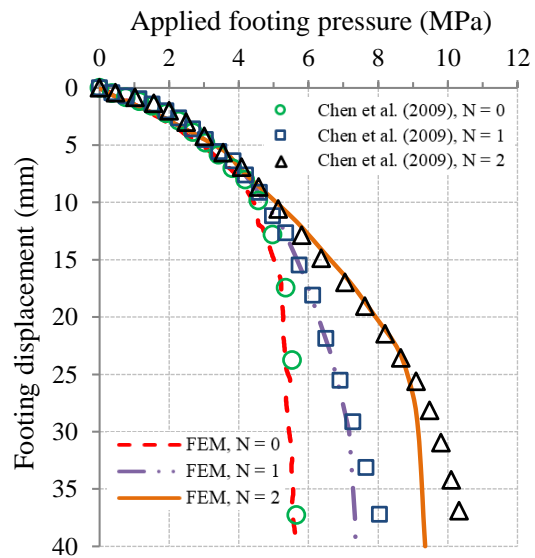


Figure 5. Load-settlement relationships for unreinforced and geogrid-reinforced soil

The problem was modeled using 8-node linear brick elements with 8 integration points (C3D8). The geogrid material model developed in the previous section is used in modeling the confined geogrid. The full geometry of the geogrid generated using over 15,300 FEs.

The crushed stone backfill was modeled using linear elasto-plastic Mohr-Coulomb failure criteria with non-associated flow rule. The input parameters are summarized in Table 2. The soil domain was discretized using C3D8 elements.

Full interlocking between the crushed limestone and the geogrid is assumed. Therefore, the geogrid-crushed limestone interaction was simulated using two fully bonded master/slave contact surfaces.

Table 2: Soil input parameters used in the in-soil FE model

Elastic Modulus E (MPa)	Poisson's ratio ν	Friction angle ϕ°	Dilatancy angle* ψ°	cohesion (MPa)
120	0.35	53	21	1E-05

*Determined using Bolton's equation [11]

To validate the proposed model, the FE results are compared with the experimental data. Fig. 5 shows the relationship between the applied footing pressure and the vertical settlement for the three investigated cases: no reinforcement ($N = 0$), one geogrid layer ($N = 1$), and two geogrid layers ($N = 2$). The load-carrying capacity generally increased when geogrid reinforcement was introduced and the ultimate bearing capacity of the footing increased with the addition of a second geogrid layer. It was found that the results obtained using the developed numerical model agreed reasonably well with the experiment data reported by Chen et al. [10].

Response of the geogrid

The deformed shapes of the geogrid layers for a given footing pressure are shown in Fig. 6. A reference pressure value of 6 MPa (smaller than the ultimate capacity for $N = 1$) was chosen as it allows for the displacements in the both cases ($N = 1$ and 2) to be examined. The vertical displacements developing in the geogrid for the investigated cases are shown in Fig. 6a and 6b. The calculated geogrid displacement decreased with the addition of a second geogrid layer. For the case of two reinforcement layers ($N = 2$), the vertical displacement of the upper geogrid layer is found to be larger than that of the lower one. Similarly, the tensile stresses in the X direction, S_{xx} , developing in the geogrid decreased when two geogrid layers were installed under the footing, as shown in Fig. 7, with the upper geogrid layer carrying more tensile stresses compared to the lower layer. In both cases, most of the geogrid deformations and stresses occurred mainly in the area immediately below the footing with very small deformation away from the loaded area.

EPS GEOFOAM INCLUSION

Expanded polystyrene (EPS) geofoam has been successfully used as a compressible inclusion in geotechnical engineering projects to induce soil strains and hence reduce earth pressures on the geotechnical structures (e.g. buried structures, retaining walls and structural slab). Using the EPS to reduce the earth loads on a buried structure installed under embankment loading is known as the induced trench installation (ITI) technique. The ITI method was originally proposed by Marston in the early 1900s and modifications were made by Spangler in 1950 to establish 'Marston-Spangler theory'. Several researches studied the relevant soil-structure interaction using numerical modelling [12-17] to help better understand the method and to address uncertainties in the design method. However, the majority of these studies have been focused on

circular or near circular sections and little work has been done to evaluate the effectiveness of the method for box culverts. The objective of the present study is to examine the role of geofoam properties in reducing earth pressure on a rigid box culvert. This is achieved using numerical analysis that allows for the effect of the EPS density to be evaluated. The numerical results are first validated using experimental data and then used to provide a new insight into the interaction between the three different elements (backfill, geofoam and culvert) of the system.

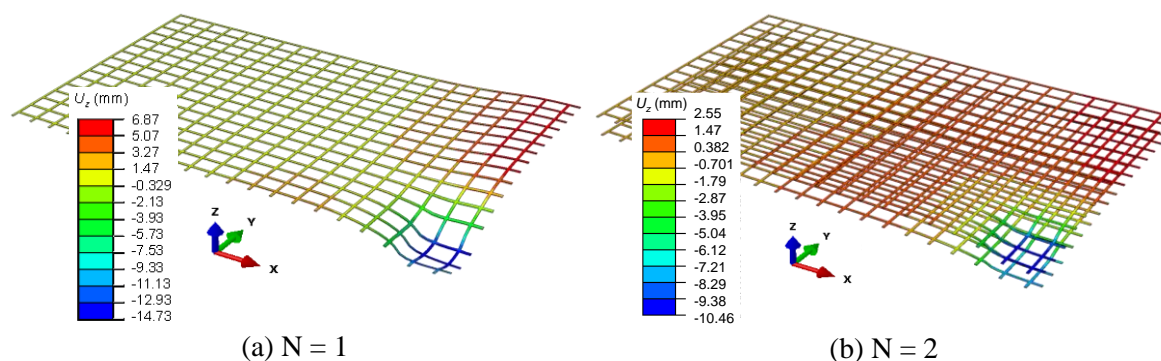


Figure 6. Geogrid deformation at a given footing load (6MPa)

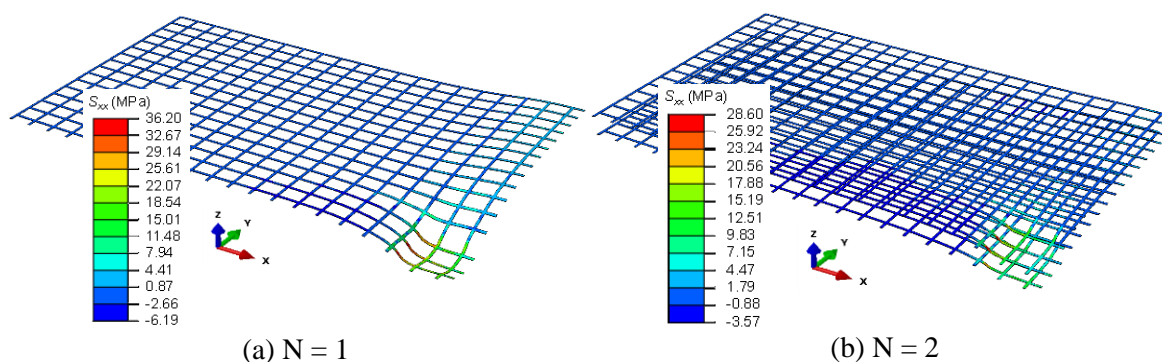


Figure 7. Tensile stresses (S_{xx}) at footing pressure of 6MPa

Modeling of Box Culvert with EPS Inclusion

The experimental results obtained by Ahmed et al. [18] are used to validate the numerical model used throughout this study. The experimental work involved the measurement of earth pressure on a square hollow structural section (HSS), with dimensions 25 cm x 25 cm x 43.5 cm and 10 mm in wall thickness, that is placed within a rigid steel chamber (1.4 m in length, 0.45 m in width and 1.2 m in height) with and without EPS block under an increased surface loading. The backfill material consisted of dry sandy gravel with unit weight of 16.3 kN/m³. The soil has a peak friction angle of 47° as obtained from direct shear tests. The backfill was placed in stages starting with a well compacted bedding layer of 25 cm in height followed by the placement of the HSS box, the side and the top backfill up to the desired height of 0.5 m above the structure. Surface pressure of up to 140kPa was applied (with constant displacement rate of 1.3 mm/min) using air bag. For the tests conducted using EPS inclusion (induced trench condition), EPS block 25 cm in width (equal to the conduit width, B), 43.5 cm in length (equal to the conduit length, L) and 50 mm in thickness is used. Throughout the experiments, the EPS block was located immediately above the culvert.

Model details and validation

The numerical models, for both the positive projecting (no EPS) and induced trench configurations, have been developed such that they follow the geometry and test procedure used in the experiments. The 2D plane strain mesh that represents the geometry of the experiment, the boundary conditions, and the different soil densities around the HSS section is shown in Figure 8. The complete mesh comprises a total number of 1962 linear plane strain elements (CPE4). The soil is modeled using linear elasto-plastic Mohr-Coulomb failure criteria with parameters as listed in Table 3.

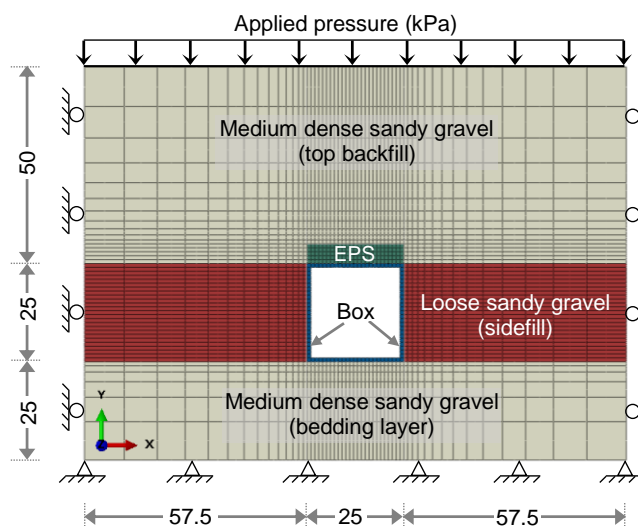


Figure 8. The FE mesh of the EPS-culvert-soil model (dimensions are in cm)

Table 3: Soil input parameters used in the EPS-culvert-soil model

Bedding and top backfill layers				
Elastic Modulus E (MPa)	Poisson's ratio ν	Friction angle ϕ°	Dilatancy angle* ψ°	cohesion (MPa)
150	0.3	47	15	1E-05
Sidefill layer				
20	0.2	30	5	1E-05

* Determined using Bolton's equation [11]

The HSS is treated as linear elastic material (density of 7850 kg/m^3) with Poisson's ratio and Young's modulus of 0.3 and 200 GPa, respectively. Three types of EPS are modeled in this study to examine the effect of geofoam density on the earth load transferred to the structure.

The EPS is modeled as nonlinear elasto-plastic strain hardening material. The elastic properties of the three EPS types are summarized in Table 4. The EPS plasticity is modeled using Mises yield criterion with isotropic hardening and associated flow rule.

Table 4. Input parameters for the elastic model of EPS material

Geofoam type	Density (kg/m^3)	E (MPa)	Poisson's ratio, ν
EPS15	14.4	4.20	0.1
EPS22	21.6	6.91	0.1
EPS39	38.4	17.8	0.15

Three different contact conditions are considered in this study; namely, i) Soil-EPS interaction, ii) Soil-BOX interaction and iii) EPS-BOX interaction. These interactions are simulated using the surface-to-surface, master/slave contact technique available in ABAQUS. Contact formulation in 2D space covers both tangential and normal directions. Boundary conditions were defined as smooth rigid along the vertical boundaries whereas the nodes at the base are fixed against displacements in both directions (rough rigid) as shown in Figure 8. After the model is generated, the initial geostatic stress condition is established by applying soil gravity and incrementally introducing the surface overburden pressure to achieve a gradual response curve.

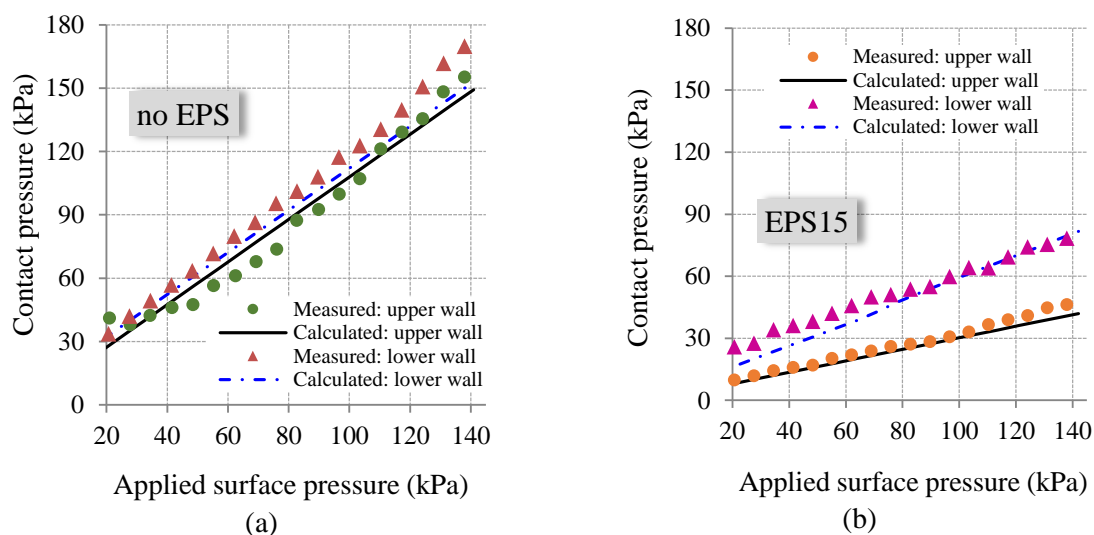


Figure 9. The EPS model validation for: a) no EPS and b) EPS15

The numerical results are first validated by comparing the calculated pressures with the measured values for two cases a) benchmark test with no geofoam and b) test using EPS15. As shown in Figure 9, the numerical model generally captured the pressure change with a reasonable accuracy at the upper and lower walls.

Effect of EPS density

The effect of EPS density is examined by comparing the calculated pressure at the investigated locations (upper, lower and side walls) for three different EPS materials, namely, EPS15, EPS22, and EPS39 (properties are given in Table 4). A surface pressure that allows for 1% EPS deformation to be achieved is used throughout this study. The results of the analysis are presented in Figure 10.

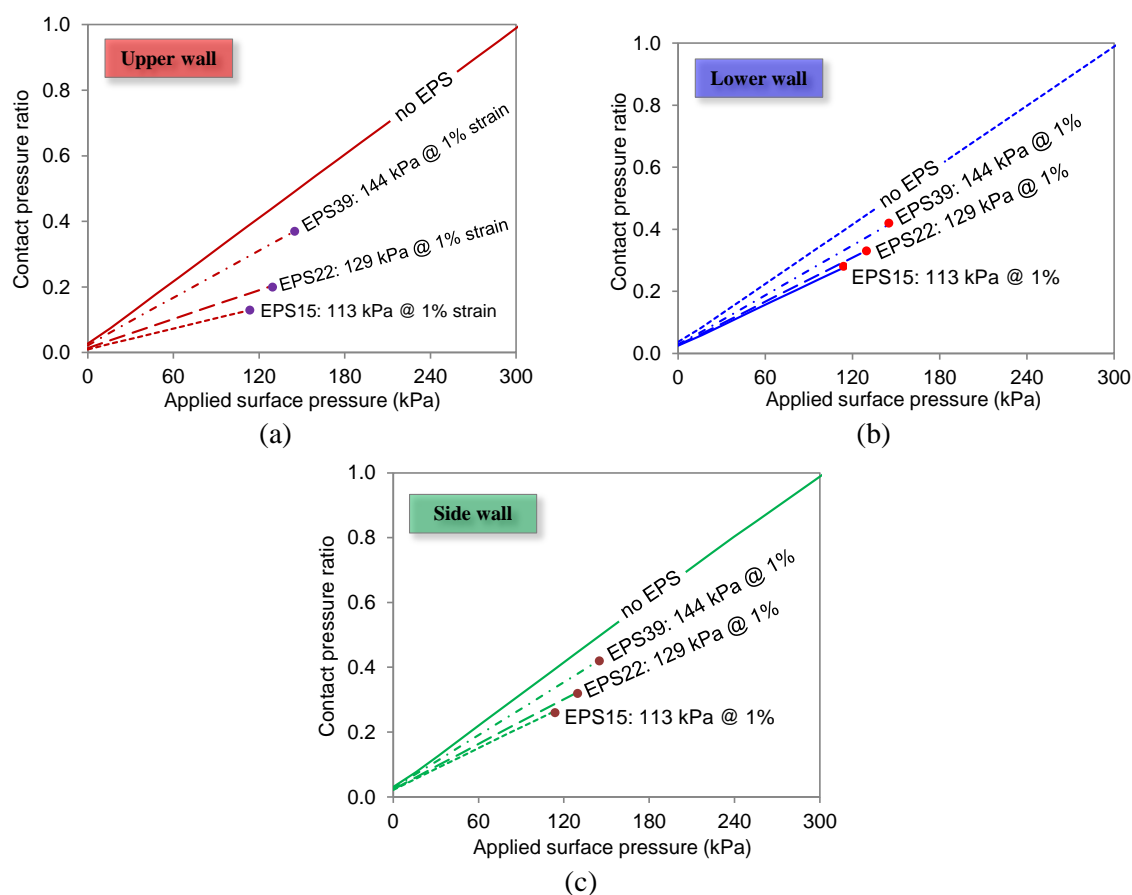


Figure 10. Effect of EPS density on the change of earth pressure on the culvert walls

For comparison purposes, the calculated pressure for each case is also compared with the benchmark analysis (no geofabric). The vertical axes in Figure 10 represent the contact pressure ratio normalized with respect to the benchmark case. For the upper wall (Figure 10a), the EPS density was found to have a significant impact on the earth pressure acting on the wall. Compared to the benchmark, the lowest contact pressure is calculated for the case of EPS15. The pressure reduction at the upper wall for different applied surface pressures (up to 1% deformation) were found to be 65%, 54% and 23% for EPS15, EPS22 and EPS39, respectively. On the lower wall, these ratios (Figure 10b) were found to be 28%, 25% and 14% for EPS15, EPS22 and EPS39, respectively. These effects are considered to be significantly smaller as compared to that calculated for the upper wall. Similar trends were found for the contact pressures on the side wall (Figure 10c) with pressure reduction ratios of 34%, 28% and 15%.

SUMMARY AND CONCLUSIONS

In this study, the finite element method is used to simulate two different classes of soil-structure interaction problems involving two types of geosynthetics. First, a procedure for the 3D FE modeling of unconfined and soil-confined geogrid is developed using ABAQUS software. A numerical model that is capable of simulating the response of unconfined biaxial geogrid under tensile loading is introduced and validated using index test results. In developing this model, the details of the geogrid

geometry is explicitly simulated. The geogrid material is represented using elastoplastic constitutive model. Tensile load applied to a geogrid specimen is carried mostly by the longitudinal ribs in the direction of the applied load and the portion carried by the junctions and transvers bars are insignificant. The displacement is distributed linearly with distance from the loaded boundary.

To confirm the validity of the unconfined geogrid model, a 3D analysis is performed to examine the geogrid performance as it interacts with the backfill material. A case study involving a square footing supported by a geogrid-reinforced crushed limestone is investigated. The 3D geometry of the geogrid, its deformation, and stress distribution were presented. The model was able to capture the 3D response of multiple geogrid layers installed under the footing. Increasing the number of geogrid layers resulted in an increase in the ultimate bearing capacity of the supporting soil. The geogrid deformations and tensile stresses for the case of $N = 1$ were found to be generally larger than those calculated for $N = 2$.

Based on the results of the numerical analyses, it can be concluded that the proposed FE approach is efficient in capturing the 3D responses of both unconfined and soil-confined geogrid and allowed for the details of the interaction between the geogrid and the surrounding backfill material to be simulated.

Another class of soil-geosynthetic interaction problems is investigated using 2D plane strain analysis to study the role of EPS inclusion above a buried box culvert in reducing the earth pressure on the walls of the structure. The developed model was used to investigate a case study of an instrumented HSS section (with and without EPS) that was placed within a rigid steel container backfilled with sandy gravel material and loaded incrementally with a vertical pressure using an air bag. The effect of the EPS density on the earth pressure acting on the HSS section was examined and found to have a significant impact on the changes in earth pressure. This study suggests that placing light weight EPS block above a rigid subsurface structure can result in a significant reduction in vertical earth pressure resulting in economic design.

ACKNOWLEDGEMENTS

This research is supported by a research grant from the Natural Science and Engineering Research Council of Canada (NSERC). The support of Plasti-Fab Ltd. throughout this study is greatly appreciated.

REFERENCES

1. Rowe RK, Mylleville BLJ. Analysis and design of reinforced embankments on soft or weak foundations. In: Bull JW, editor. Soil-Structure Interaction: Numerical Analysis and Modelling: Chapman & Hall; 1994. p. 231-60.
2. Sugimoto M, Alagiyawanna A. Pullout Behavior of Geogrid by Test and Numerical Analysis. Journal of Geotechnical and Geoenvironmental Engineering. 2003;129(4):361-71.
3. Yogarajah I, Yeo KC. Finite element modelling of pull-out tests with load and strain measurements. Geotextiles and Geomembranes. 1994;13(1):43-54.
4. Perkins SW, Edens MQ. Finite element modeling of a geosynthetic pullout test. Geotechnical and Geological Engineering. 2003;21(4):357-75.

5. McDowell G, Harireche O, Konietzky H, Brown S, Thom N. Discrete element modelling of geogrid-reinforced aggregates. Proceedings of the ICE-Geotechnical Engineering. 2006;159(1):35-48.
6. Hussein MG, Meguid MA, editors. Three-Dimensional Finite Element Analysis of Soil-Geogrid Interaction under Pull-out Loading Condition. GeoMontreal, 66th Canadian Geotechnical Conference; 2013 29 Sep.-03 Oct.; Montreal, Quebec, Canada: Canadian Geotechnical Society.
7. Tran VDH, Meguid MA, Chouinard LE. A finite-discrete element framework for the 3D modeling of geogrid-soil interaction under pullout loading conditions. Geotextiles and Geomembranes. 2013;37:1-9.
8. Tran VDH, Meguid MA, Chouinard LE, editors. The application of coupled finite-discrete element method in analyzing soil-structure interaction problems. 3rd International Conference on Particle-Based Methods Fundamentals and Applications, Particles 2013; 2013; Stuttgart.
9. ABAQUS User's Manuals, Version 6.13, Dassault Systems Simulia Corp., Providence, RI, USA. ABAQUS, 2013.
10. Chen Q, Abu-Farsakh M, Sharma R. Experimental and Analytical studies of reinforced crushed limestone. Geotextiles and Geomembranes. 2009;27(5):357-67.
11. Bolton MD. The strength and dilatancy of sands. Géotechnique. 1986; 36:65-78.
12. Kim K, Yoo CH. Design Loading for Deeply Buried Box Culverts. Report No. IR-02-03., 215 pp., Alabama, USA: Highway Research Center, Auburn University, 2002.
13. Kang J, Parker F, Kang YJ, Yoo CH. Effects of frictional forces acting on sidewalls of buried box culverts. International Journal for Numerical and Analytical Methods in Geomechanics. 2008;32(3):289-306.
14. McAfee RP, Valsangkar AJ. Field performance, centrifuge testing, and numerical modelling of an induced trench installation. Canadian Geotechnical Journal. 2008;45(1):85-101.
15. Sun C, T.C. H, Benkham TL. Reduction of stresses on buried rigid highway structures using the imperfect ditch method and expanded polystyrene (geofoam) Report No. KTC-07-14-SPR-228-01-1F, 49 pp., Kentucky, USA: Kentucky Transportation Center, University of Kentucky, 2009.
16. McGuigan BL, Valsangkar AJ. Centrifuge testing and numerical analysis of box culverts installed in induced trenches. Canadian Geotechnical Journal. 2010;47(2):147-63.
17. McGuigan BL, Valsangkar AJ. Earth pressures on twin positive projecting and induced trench box culverts under high embankments. Canadian Geotechnical Journal. 2011;48(2):173-85.
18. Ahmed MR, Meguid M, Whalen J. Laboratory Measurement of the Load Reduction on Buried Structures overlain by EPS Geofoam. The 66th Canadian Geotechnical Conference; Montreal, Canada, . Paper No. 217 (8 pages)2013.